Journal of Marine Science and Application (2023) 22: 102-114
https://doi.org/10.1007/s11804-023-00319-9

RESEARCH ARTICLE

Numerical Study of Green Water on a Tumblehome Vessel in Strong Nonlinear Regular Waves

Baikang Sun[1], Binbin Zhao[1], Yang Xu[2], Shan Ma[1] and Wenyang Duan[1]

Received: 26 October 2022 / Accepted: 02 January 2023

Abstract

Owing to the large amplitude and nonlinearity of extreme sea waves, sailing ships exhibit obvious large-amplitude motion and green water. For a tumblehome vessel, a low-tumblehome freeboard and wave-piercing bow make green water more likely. To study the green water of a wave-facing sailing tumblehome vessel in strong nonlinear regular waves, the computational fluid dynamics software STAR-CCM+ was used. The Reynolds-averaged Navier–Stokes method was used for the numerical simulation, and the *k*-epsilon model was adopted to deal with viscous turbulence. The volume of the fluid method was used to capture the free surface, and overset grids were utilized to simulate the large-amplitude ship motion. This study delves into the influence of wave height on the ship motion response and a tumblehome vessel green water under a large wave steepness ($0.033 \leqslant H/\lambda \leqslant 0.067$) at $Fr = 0.22$. In addition, the dynamic process of green water and the "wave run-up" phenomenon were evaluated. The results suggest that when the wavelength is equal to the ship length and the wave steepness increases to 0.056, the increase in the water height on the deck is obvious. However, the wave height had little effect on the green water duration. The wave steepness and "backwater" have a great impact on the value and number of the peak of the water height on the deck. When the wave steepness exceeded 0.056, the water climbed up, and the plunging-type water body was formed at the top of the wave baffle, resulting in a large water area on the deck.

Keywords Tumblehome vessel; Green water; Impact loads; Wave run-up; Strong nonlinear regular waves

1 Introduction

Ships inevitably encounter extreme waves while sailing. In severe sea conditions, a large amount of seawater rushes onto the deck, and huge impact loads cause damage to the equipment and superstructures on the deck. Moreover, green water can even cause hull capsizing.

For a tumblehome vessel, such as the DDG1000 in the USA, the distinct attributes of this hull form are a low-tumblehome freeboard and a wave-piercing bow. These novel shape designs can effectively reduce ship resistance in waves and improve stealth performance. However, an inversely inclined bow makes the hull motion violent, which easily causes green water. Therefore, it is essential to accurately predict and study the tumblehome vessel green water during strong nonlinear regular waves.

In previous studies, green water has predominantly been studied using experimental and theoretical methods. Tasaki (1960) concluded from experiments that green water in regular waves is caused by the relative motion of bows and waves. Berhault et al. (1998) found that the water height on the deck is related to the bow shape and drift angle. Stansberg (2001) measured the relative motion of a floating production storage and offloading (FPSO) unit and the green water impact pressure.

With the improvement of the test technology, to be closer to extreme sea waves in the real ocean, researchers have

Article Highlights

- Motion response, water height on deck, and impact loads were evaluated under different large wave steepness;
- The influence of wave height on "wave run-up" and water volume on the deck in an encounter period was evaluated;
- The results provide a reference for green water prediction in tumblehome vessels under strong nonlinear regular waves.

✉ Binbin Zhao
zhaobinbin@hrbeu.edu.cn

[1] College of Shipbuilding Engineering, Harbin Engineering University, Harbin 150001, China

[2] School of Ocean Engineering and Technology, Sun Yat-sen University, Zhuhai 519082, China

paid great attention to green water under high-sea conditions. Duan et al. (2013) studied the relationship between the drift and impact pressure of an S-175 ship under high-sea conditions. Gao et al. (2016) evaluated the trim attitude influence on green water under different wave steepness values ($[H/\lambda]_{max}$ = 0.13). Rosetti et al. (2019) verified the applicability of the computational fluid dynamics (CFD) method for predicting FPSO green water in beam waves with large wave steepness ($[H/\lambda]_{max}$ = 0.08). Deng et al. (2021) evaluated the evolution of "plunging" green water of an FPSO through experiments ($[H/\lambda]_{max}$ = 0.10). The green water model test is the most reliable method and provides an important reference for numerical calculations.

In terms of the theory method, Ochi (1964) used linear hydrodynamic theory and probability statistics to evaluate green water. He et al. (1996) and Wang and Wu (1998) improved this method and quantitatively evaluated the severity of green water pollution. Ogawa et al. (1997) evaluated the impact loads and water height on a deck during irregular waves using probability statistics. However, accurately evaluating impact loads utilizing probability statistics is challenging. The linear theory cannot deal with green water in strong nonlinear waves.

Based on the potential flow, dam-break (Goda et al. 1976), and flood wave theories (Ogawa et al. 1998), and fully nonlinear boundary element method (Greco 2001) have been proposed to numerically solve green water. However, the potential flow theory overlooks fluid viscosity. It is difficult to simulate strong nonlinear phenomena, including wave breaking, plunging jets, and splashing around ship hulls in extreme waves.

In recent years, CFD methods have been vastly utilized for green water numerical simulation under large wave steepness.

Liang et al. (2010) and Gong et al. (2014) studied green water using a dynamic grid and the volume of fluid (VOF) method in Fluent. Liu (2017) and He et al. (2018) evaluated the influence of wave amplitude and wavelength on the green water of ships. Liu (2017) focused on the "wave run-up" and the total volume of water on the tumblehome hull DTMB5613's deck under a large wave steepness ($[H/\lambda]_{max}$ = 0.05). He et al. (2018) used the FINE/Marine software to evaluate the green water dynamic process of a wave-facing sailing Wigley ship ($[H/\lambda]_{max}$ = 0.027). Xu and Tang (2018) evaluated the influence of air entrainment on green water. Liu and Li (2020) studied the use of green water for freak waves. Yang et al. (2021) evaluated the influence of velocity field change on the point pressure at the FPSO deck and the overall stress of the structure during green water.

Currently, most CFD numerical studies have investigated the green water of conventional ship types with wave steepness less than 0.05, and few studies have focused on the tumblehome vessels' green water attributes in extreme sea waves. A large wave steepness can affect the ship motion and green water severity. Therefore, it is essential to study the effect of large wave steepness > 0.05 on the tumblehome vessel green water.

In this study, the commercial CFD software Star-CCM+ was used to simulate the green water of wave-facing sailing tumblehome vessels in strong nonlinear regular waves. The predicted water height on the deck and slamming pressure were compared with experimental data to verify the reliability of the CFD method. When the wave steepness exceeded 0.05, the influence of the wave height on green water was evaluated. This study focuses on the dynamic process of green water and the "wave run-up" phenomenon to further evaluate the green water mechanism of tumblehome vessels under large wave steepness.

2 Numerical methods of green water

2.1 Governing equation

The numerical simulation of the tumblehome vessels' green water was based on the CFD commercial software Star-CCM+. The fluid was presumed viscous and incompressible. The governing equations are as follows.

$$\nabla \cdot \boldsymbol{U} = 0 \tag{1}$$

$$\frac{\mathrm{D}\boldsymbol{U}}{\mathrm{D}t} = \boldsymbol{f} - \frac{1}{\rho}\nabla p + \boldsymbol{v}\nabla^2\boldsymbol{U} \tag{2}$$

where $\boldsymbol{U}$ is the velocity field vector, ρ is the fluid density, p is the pressure, and v is the kinematic viscosity coefficient. Eq. (1) represents the continuity equation of incompressible viscous fluid. Eq. (2) represents the Navier–Stokes (N–S) equation of incompressible viscous fluid.

Each term in the N–S equation represents a force acting on the fluid of unit mass. $\frac{\mathrm{D}\boldsymbol{U}}{\mathrm{D}t}$ represents the inertial force; $\boldsymbol{f}$, $-\frac{1}{\rho}\nabla p$, and $v\nabla^2\boldsymbol{U}$ represent the mass force, resultant force of pressure, and viscous force, respectively.

In this study, the Reynolds-averaged Navier–Stokes (RANS) method was used to solve the N–S equation. The K-epsilon model was selected for viscous turbulence.

2.2 VOF method

The interface between water and air is captured using the VOF method. The definition of the ith phase volume fraction is given as follows:

$$\alpha_i = \frac{V_i}{V} \tag{3}$$

where V_i is the volume of the ith phase in the cell, V is the total cell volume, and α_i is the relative proportion of the

fluid in each cell, as depicted in Eq. (4).

$$\begin{cases} \alpha_i = 0\,; & \text{air} \\ \alpha_i = 1\,; & \text{water} \\ 0 < \alpha_i < 1\,; & \text{interface} \end{cases} \tag{4}$$

where $\alpha_i = 0$ means that the cell is full of air, $\alpha_i = 1$ means that the cell is full of water, and $0<\alpha_i<1$ means that the cell is at the free surface.

2.3 Wave generation

To simulate regular head waves with large wave steepness, 5th-order Stokes waves were adopted at the inlet boundary to generate waves. According to the 5th-order Stokes wave theory in infinite deep water (Fenton 1985), the wave surface elevation $\eta(x,t)$ is defined as

$$\begin{aligned} \eta(x,t) = A\cos\theta + \frac{1}{2}kA^2\cos 2\theta - \frac{3}{8}k^2A^3(\cos\theta - \cos 3\theta) \\ + \frac{1}{3}k^3A^4(\cos 2\theta + \cos 4\theta) \\ + k^4A^5\left(-\frac{422}{384}\cos\theta + \frac{297}{384}\cos 3\theta + \frac{125}{384}\cos 5\theta\right) \end{aligned} \tag{5}$$

The encounter frequency ω_e in the regular head wave condition is defined by the dispersion relation:

$$\begin{aligned} \omega_e &= \omega + kU_{\text{ship}} \\ &= \sqrt{gk(1 + k^2A^2 + k^4A^4)} + kU_{\text{ship}} \end{aligned} \tag{6}$$

where $A = H/2$, $\theta = kx - \omega_e t$, H is the wave height, k is the wave number, ω is the frequency of the wave, and U_{ship} is the ship velocity.

2.4 Wave damping based on the Euler overlay method

The wave forcing function provided in STAR-CCM+ was used for wave damping based on the Euler overlay method (EOM) theory (Kim et al. 2012; Baquet et al. 2017).

The finite-volume formulation of the diffusion-transport equation of a scalar function ϕ within a volume V surrounded by the boundary surface A is given by

$$\frac{\mathrm{d}}{\mathrm{d}t}\int_V \rho\phi\,\mathrm{d}V + \int_A \rho\phi\left(\boldsymbol{v} - \boldsymbol{v}_g\right)\cdot\mathrm{d}\boldsymbol{a} = \int_A \Gamma\nabla\phi\cdot\mathrm{d}\boldsymbol{a} + \int_V S_\phi\mathrm{d}V \tag{7}$$

where ρ is the density, $\boldsymbol{v}$ denotes the fluid velocity vector, $\boldsymbol{v}_g$ denotes the fluid mesh velocity vector, $\boldsymbol{a}$ is the area vector on the boundary surface A, Γ is the diffusion parameter, and S_ϕ is the source term for the scalar. The scalar function ϕ can be the velocity or volume fraction depending on whether Eq. (7) describes the conservation of momentum or phase.

In the EOM, an additional source term is added to each conservation equation to achieve forced wave absorption. The new source term S_ϕ^* in Eq. (7) is given by

$$S_\phi^* = S_\phi - \gamma\rho(\phi - \phi^*) \tag{8}$$

where γ is the forcing function, ρ is the fluid density, ϕ is the current solution to the transport equation, and ϕ^* is the solution forced by the EOM.

The expression for the forcing function γ is given by

$$\begin{cases} \gamma(x) = 0\,; & \text{for x at the inner zone} \\ \gamma(x) = \gamma_{\max}\cos^2(\pi x/2l)\,; & 0 < x \leqslant l \\ \gamma(x) = \gamma_{\max}\,; & x = 0 \end{cases} \tag{9}$$

where $\gamma_{\max}$ is the maximum value of $\gamma(x)$, and l is the ramping length of the forcing function.

Figure 1 shows the top view of the computational domain and the sketch of the forcing function. The green and red contour lines represent the inner and outer boundaries, respectively.

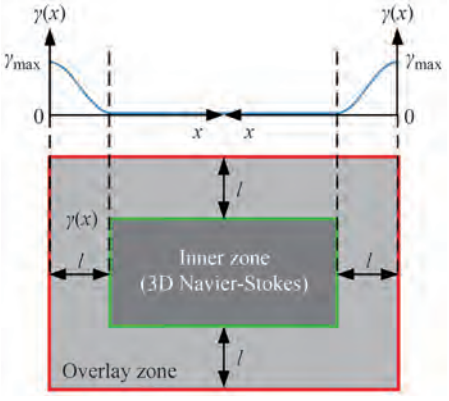

Figure 1 Schematic sketch for the forcing function definition in the EOM

The N–S equation was solved in the inner zone, where the forcing function γ is 0. In the overlay zone with a width of l, $\gamma(x)$ smoothly increases from 0 at the inner boundary to $\gamma_{\max}$ at the outer boundary, as depicted in Figure 1. Then, the discretized N–S equation solution is forced to move to the theoretical or a simplified numerical solution.

The wave forcing function based on the EOM can reduce the size of the computing domain to effectively shorten the solution time. In addition, it can eliminate the surface wave reflection problem at the boundary.

3 Model and simulation conditions

3.1 Geometric model

A tumblehome vessel model was used for all numerical

simulations. The geometric model is depicted in Figure 2, and its principal dimensions are listed in Table 1. A wave baffle was inclined to the stern at an angle of 20° at the 8th station, as depicted in Figure 3.

Figure 2 Geometry of the tumblehome vessel

Table 1 Main tumblehome vessel parameters

Parameters	Symbol	Full scale	Model
Scale	-	1	1/40
Waterline length	L_{wl} (m)	180	4.5
Waterline breadth	B_{wl} (m)	21	0.525
Draft	T (m)	7	0.175
Displacement	Δ (t)	14 000	0.213 4
Vertical center of gravity (from keel)	Z_{CG}	7.8	0.195
Longitudinal center of gravity (from midship, fwd+)	X_{CG}	−3.3	−0.083

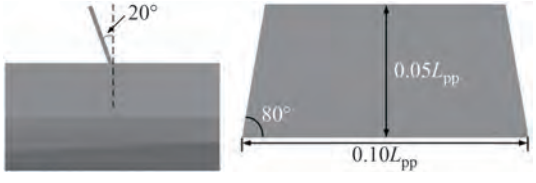

Figure 3 Dimension of the wave baffle (superstructure)

Wave probes PH1–PH6 and measuring points B1–B7 were used to measure the water height on the deck and slamming pressure on the hull surface, as depicted in Figures 4 and 5.

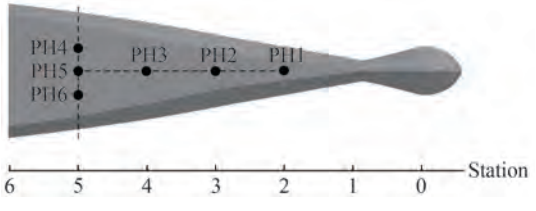

Figure 4 Wave probes of the water height on the deck

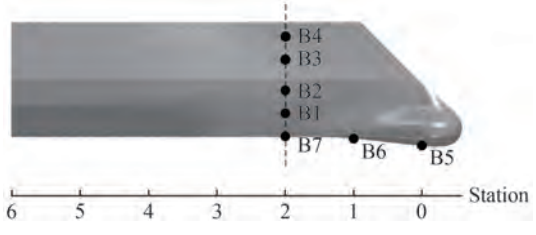

Figure 5 Measuring points of the slamming pressure

The origin of the Earth-fixed coordinate system is located at the keel in the midship. The *X*-axis is in the longitudinal direction from the stern to the bow, *Y*-axis is in the portside direction, and the *Z*-axis is vertically upward. The ship hull is divided into 20 stations. The 0th station is at the bow, and the 10th station is at the midship.

Table 2 enlists the detailed positions of PH1−PH6 and B1−B7 in the Earth-fixed coordinate system. PH4 and PH6 are symmetrical about the midship plane.

Table 2 Positions of PH1–PH5 and B1–B7

Point No.	Station	X/L_{wl}	Y (m)	Z (m)
PH1	2	0.40	0	0.375
PH2	3	0.35	0	0.375
PH3	4	0.30	0	0.375
PH4	5	0.25	0.075	0.375
PH5	5	0.25	0	0.375
B1	2	0.40	−0.031	0.075
B2	2	0.40	−0.065	0.150
B3	2	0.40	−0.062	0.250
B4	2	0.40	−0.043	0.325
B5	0	0.50	0	−0.291
B6	1	0.45	0	−0.005
B7	2	0.40	0	0

The ship is free to heave and pitch during the simulation. The origin of the ship-fixed coordinate system is located at the ship's center of gravity. The directions of the ξ-axis, η-axis, and ζ-axis are consistent with those of the *X*-axis, *Y*-axis, and *Z*-axis of the Earth-fixed coordinate system.

The wave probes (PH1−PH6) were set in the ship-fixed coordinate system during the ship motion, as depicted in Figure 6, to ensure the relative position of the wave probes and so that the ship remains unchanged. The water height on the deck is defined as H_{GW} (height of the green water):

$$H_{GW} = \zeta_{GW} - \zeta_{Deck} \tag{10}$$

where ζ_{GW} is the water height relative to the ζ-axis, $\zeta_{Deck} = Z_{Deck} - Z_{CG} = 0.18$, and ζ_{Deck} is the height of the deck relative to the ζ-axis. Z_{Deck} and Z_{CG} are the height of the deck and center of gravity relative to the *Z*-axis, respectively.

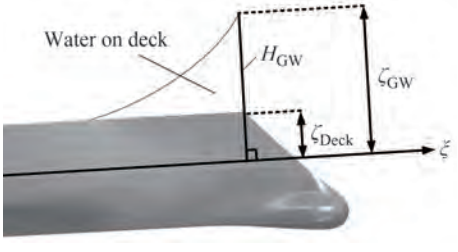

Figure 6 Schematic sketch for the water height on the deck

3.2 Simulation conditions

The numerical simulations were performed in regular head waves with different wave heights for the tumblehome vessel advancing at Fr = 0.22. The wave steepness H/λ ranged from 0.033 to 0.067.

The simulation conditions are summarized in Table 3, where T is the period of the wave, Te is the encounter period based on the unlimited-depth 5th-Stokes wave theory (see Eq. (6)), λ is the wavelength, H is the wave height, and Fr is the Froude number, defined as:

$$Fr = \frac{U_{\text{ship}}}{\sqrt{gL_{\text{wl}}}} \tag{11}$$

where U_{ship} is the velocity of the ship, g is the acceleration of gravity, and L_{wl} is the waterline length of the ship.

Table 3 Simulation conditions

Case No.	Fr	T (s)	Te (s)	λ/L_{wl}	H (m)	H/λ
1	0.22	1.688	1.091	1.0	0.150	0.033
2		1.677	1.086		0.225	0.050
3		1.672	1.084		0.250	0.056
4		1.661	1.079		0.300	0.067

4 Numerical validation

4.1 Numerical wave-generating validation

A numerical "forced wave tank" was established using the wave forcing function in the STAR-CCM+ software to simulate regular waves with large wave steepness.

The 5th-order Stokes wave was adopted to simulate regular waves with a 0.08 wave steepness. The water depth, wave height, and wavelength were 9, 0.36, and 4.5 m, respectively.

According to the EOM, the velocity inlet with wave forcing was used on all vertical boundaries. The ramping length of the forcing function was set to L_{wl}. The pressure outlet was used on the top, and the velocity inlet was used on the bottom.

To ensure the accuracy of the wave simulation, a 2$^{\text{nd}}$-order scheme was adopted for the time step. The CFL number is less than 0.5 on the free surface, defined as

$$\text{CFL} = \frac{C_{\text{wave}} \cdot \text{d}t}{\text{d}x} \tag{12}$$

where C_{wave} is the phase velocity of regular waves, dt is the time step, and dx is the horizontal cell dimension of the free surface region.

20–40 cells were within the wave height range. 80–160 cells were set within the wavelength range. The maximum aspect ratio of the grid element on the free surface $\Delta z/\Delta x$ was 1/8. The grid refinement is depicted in Figure 7.

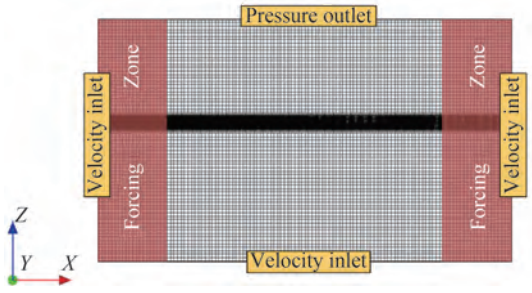

Figure 7 Boundary conditions and grid refinement of the "forced wave tank"

The predicted numerical wave height was compared with the solution of the stream function theory, as depicted in Figure 8, where t is the simulation time, and T is the period of the wave.

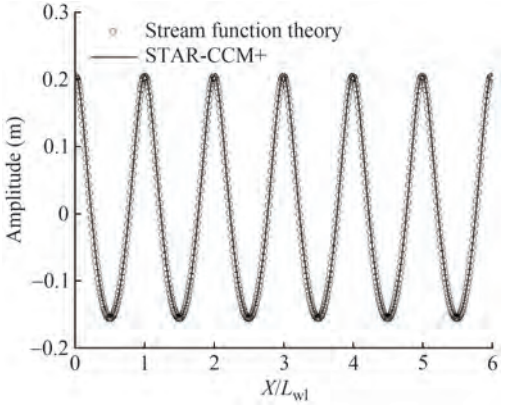

Figure 8 Wave height in the whole domain

The numerical wave height in the entire computational domain at t/T = 15 almost coincided with the theoretical solution of the stream function, as depicted in Figure 8.

Figure 8 depicts that the CFD strategy for wave generation can provide accurate information on regular waves with large wave steepness ($H/\lambda \leqslant 0.08$).

4.2 Domain and boundary conditions

Half of the ship model was used for the numerical simulation. The computational domain size was set as follows: The inlet boundary was located at $2L_{\text{wl}}$ from the front perpendicular, and the outlet boundary was located at $3L_{\text{wl}}$ from the after perpendicular. The top and bottom boundaries were located at $1.5L_{\text{wl}}$ and $2L_{\text{wl}}$, respectively. The lateral boundary was located $2L_{\text{wl}}$ away from the midship plane, as depicted in Figure 9.

The boundary conditions were set up as follows: The velocity inlet with wave forcing was used on the inlet, outlet,

bottom, and side wall; there was no-slip wall condition on the ship hull; pressure outlet was utilized on the top; and the symmetry condition was located at the symmetry plane, as depicted in Figure 9.

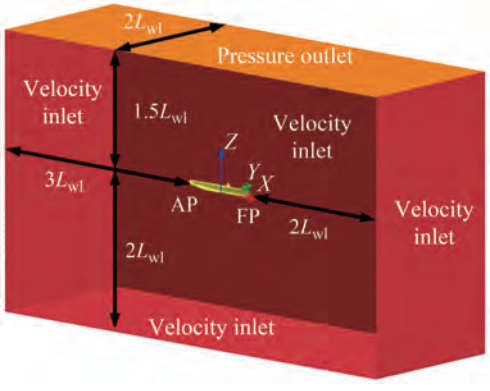

Figure 9 Computational domain and boundary conditions

4.3 Mesh convergence studies on green water

Trimmed meshes were generated using STAR-CCM+. Overset grids were adopted to accurately simulate large-amplitude ship motions in regular waves. A convergence study for the mesh size was conducted in Case 2. Coarse (Mesh 1), medium (Mesh 2), and fine (Mesh 3) grids correspond to the total cell numbers of 2.85, 3.94, and 5.66 million, respectively. The CFL number is 0.5.

The mesh refinement of the background, overlap, overset and free surface regions of Mesh 1 is depicted in Figure 10.

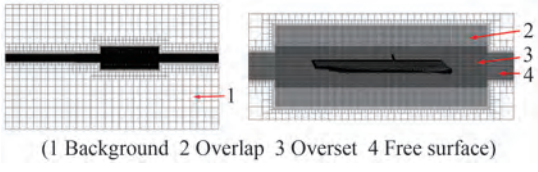

Figure 10 Side view of the mesh refinement of Mesh 1

The mesh refinement strategy is the same for the three meshes. The percentage of the grid size relative to the base size in each region is summarized in Table 4. The total cell numbers are changed by resizing the size of the base size. Mesh 1, Mesh 2, and Mesh 3 correspond to the base sizes of $L_{wl}/65$, $L_{wl}/80$, and $L_{wl}/100$, respectively.

The grid size of each region is summarized in Table 4.

Table 4 Grid refinement of each region

Block name	No.	dx/Basic size (%)	dy/Basic size (%)	dz/Basic size (%)
Background	1	800	800	800
Overlap	2	50	200	25
Overset	3	50	100	12.5
Free surface	4	100	400	12.5

The sensitivity of the water height on the deck and slamming pressure to the grid scale was analyzed. The water height on the decks of PH2 and PH4 under different mesh sizes is depicted in Figure 11. H_{GW} is the water height on the deck (see Eq. (10)), and t is the simulation time.

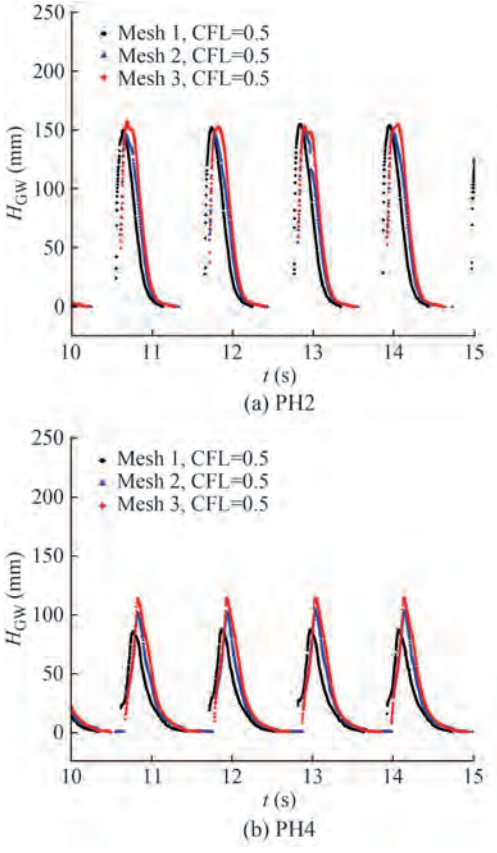

Figure 11 Mesh convergence of the water height on the deck

Figure 11(a) depicts that with an increase in the total cell number of meshes, the crest of the water height on the deck is basically unchanged at PH2. The three meshes had a slight phase difference. Figure 11(b) depicts that the predicted crest of the water height on the deck of Mesh 1 is lower than those of Mesh 2 and Mesh 3. The time history curves of Mesh 2 and Mesh 3 basically coincide at PH4.

The results show that the grid size mainly affects the simulation accuracy of the water height on the deck at the station, which is far from the ship bow in the green water.

The slamming pressures of B2 and B6 under different mesh sizes are depicted in Figure 12. P_{GW} is the dynamic pressure of slamming, and t is the simulation time.

Figure 12 depicts that with an increase in the total cell number of the mesh, the crest of the slamming pressure is basically unchanged at B2 and B6. Mesh 1 has an obvious phase difference. The time histories of Mesh 2 and Mesh 3 basically coincide.

By comprehensively comparing the time history with different total cells, it is considered that Mesh 2 converged.

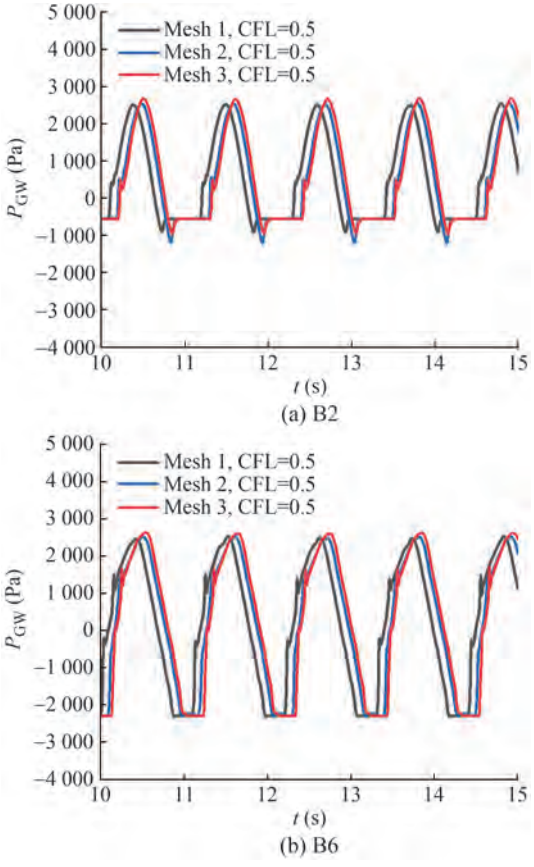

Figure 12 Mesh convergence of the slamming pressure

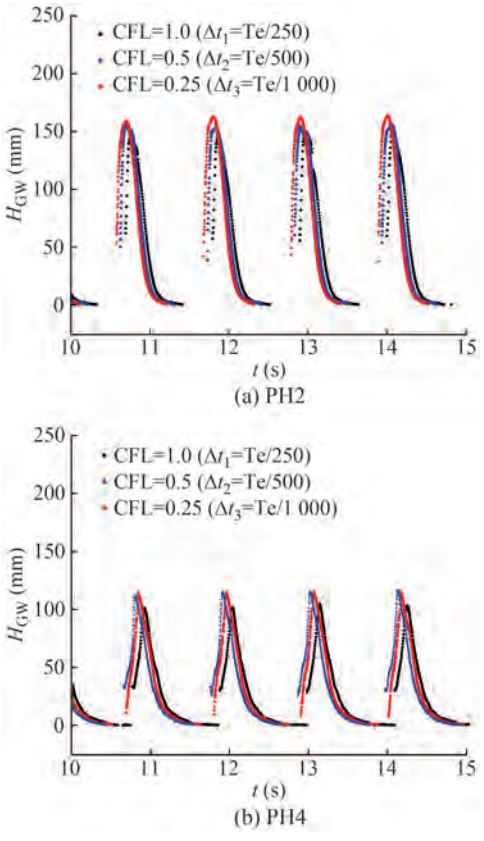

Figure 13 Time step convergence of the water height on the deck

4.4 Time step convergence studies on the green water

A convergence study for the time step was conducted in Case 2 using the medium grid (Mesh 2). Coarse (Δt_1), medium (Δt_2), and fine (Δt_3) time steps correspond to Te/2^8 (CFL = 1.0), Te/2^9 (CFL = 0.5), and Te/2^{10} (CFL = 0.25), respectively.

The water height on the decks of PH2 and PH4 under different time steps is depicted in Figure 13. The slamming pressure of B2 and B6 under different time steps is depicted in Figure 14.

Figures 13 and 14 depict the predicted crest of the water height on the deck, and the slamming pressure of Δt_1 is lower than that of Δt_2 and Δt_3. The time histories of Δt_2 and Δt_3 basically coincide.

The results show that when the CFL number is greater than 0.5, the predicted water height on the deck and slamming pressure will be lower. The comparison of the time history with different time steps shows that Δt_2 converged.

The comparison of the time history with different time steps shows that Δt_2 converged.

4.5 Green water validation

The convergent numerical results of the water height on

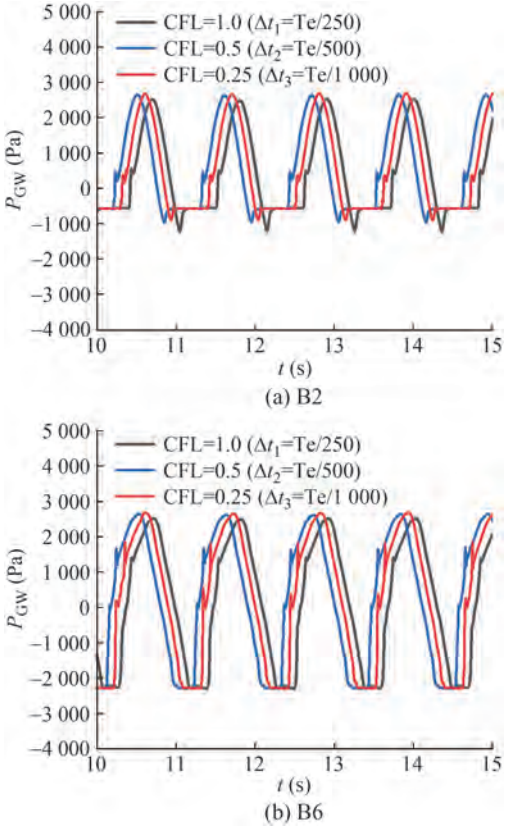

Figure 14 Time step convergence of the slamming pressure

the deck and slamming pressure in Case 2 (Fr = 0.22, H/λ = 0.050) were selected for comparison with the experimental data (Sun et al. 2017; Li et al. 2020).

The computed time history of the water height on the deck at PH1–PH5 and the slamming pressure at B1–B7 was compared with the measurements in Case 2, as shown in Figure 15.

Figure 15 demonstrates that the predicted water heights on the deck at PH2–PH5 are in good agreement with the test results. The predicted crest value at PH1 after 32 s is much lower than the experimental results. This is due to the large movement of the bow during the experiment, resulting in a certain error in the measurement of the water height on the deck at PH1.

Figure 16 depicts a good agreement between the experimental results and the predicted slamming pressure at B1–B7.

In general, the predicted water height on the deck and the slamming pressure at each measuring point on the bow agree with Case 2 test results. Hence, the CFD numerical strategy was accurate and reliable for simulating tumblehome vessel green water under large steepness waves.

5 Results and discussion

5.1 Influence of the wave height on ship motions

The four cases in Table 3 were selected to evaluate the influence of wave height on the ship motion response. The time history of the ship motion with different wave heights is depicted in Figure 17.

Figure 17(a) depicts the heave motion at different wave heights. When H/λ changed from 0.050 to 0.056, the heave motion amplitude increased most significantly. Compared to Case 2, the trough and crest values increased by 31.25% and 30.37%, respectively, in Case 3. The sinkage in Case 4 increased by 11.23%, whereas the amplitude of the rise changed only by a little compared with Case 3.

Figure 17(b) depicts the pitch motion at different wave heights. Compared with Case 2, the trim amplitude by the bow increased by 14.57% in Case 3. Compared with Case 3, the trim amplitude by the bow in Case 4 increased by 10.27%.

Thus, for a wave-facing tumblehome vessel, when H/λ increases to 0.056, a large-amplitude heave motion will occur. When H/λ increased to 0.067, the increase in sinkage was significant. The influence of the wave height on the pitch motion is predominantly reflected in the trim change by the bow.

5.2 Influence of the wave height on the water height on the deck

The time history of the water height on the deck of the PH1 and PH3 wave height gauges at different wave heights is depicted in Figure 18.

Figure 18(a) depicts that with an increase in the wave height, the water height on the deck gradually increases at PH1. Figure 18(b) depicts that the water height on the deck increased most obviously in Case 2 at PH3, and compared with Case 1, the crest value increased by 62 mm. However,

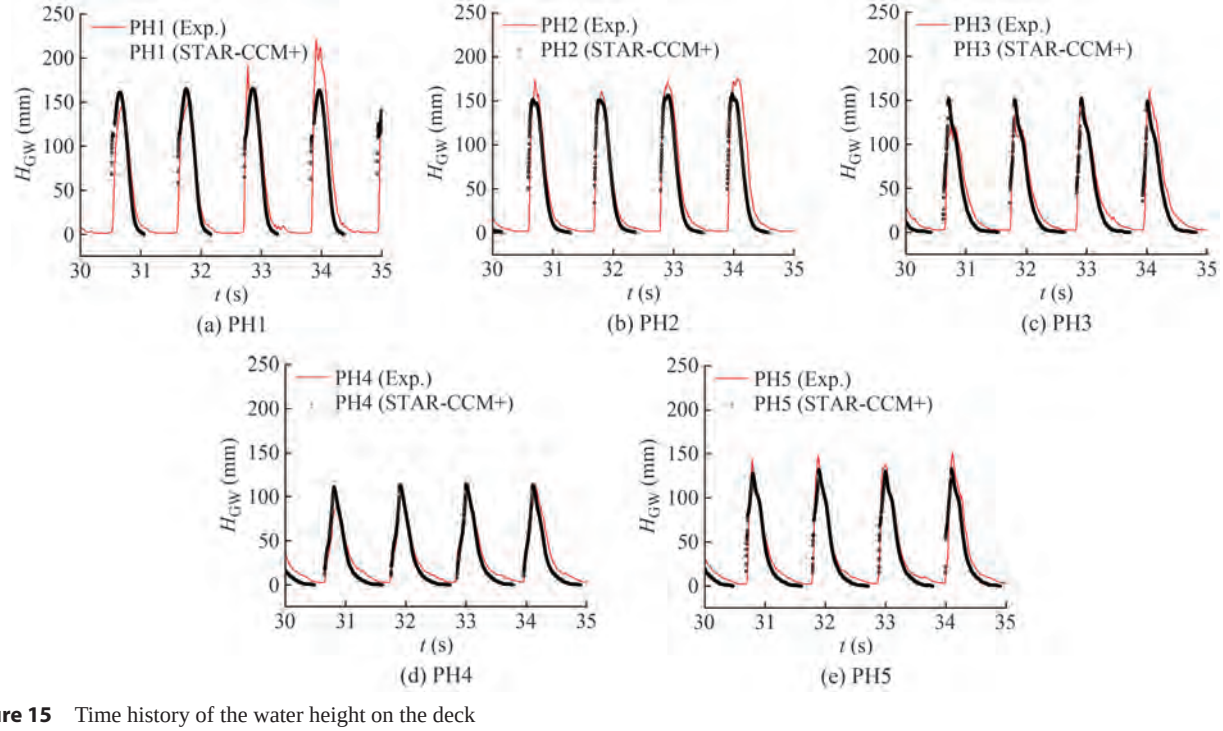

Figure 15 Time history of the water height on the deck

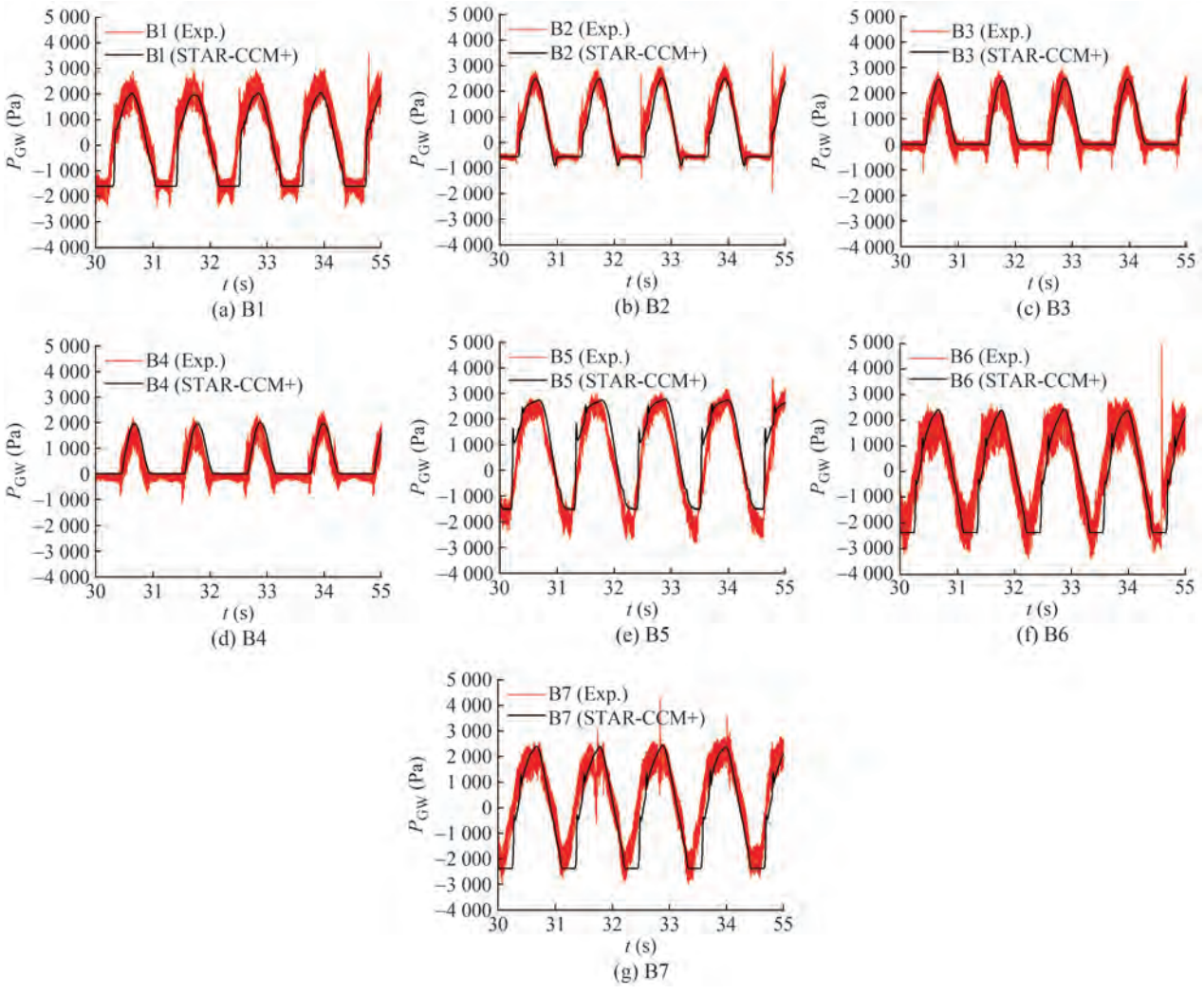

Figure 16 Time history of the slamming pressure

the wave height had little effect on the green water duration at PH1 and PH3.

In Figure 18(b), an interesting phenomenon is observed. The water height on the deck of Case 1 has one significant peak at PH3. However, there are two peaks in Case 2, Case 3, and Case 4. The value of the first peak is larger than that of the second peak in Case 2 and Case 3. The value of the first peak is smaller than that of the second peak in Case 4.

This is because in the last encounter period, during the "wave run-up" process, a part of the water attached to the wave baffle returned to the deck, and accumulated water formed from the wave baffle to the bow. This part of the water body, "backwater," participates in the green water process in the current encounter period.

When the wave steepness was small, due to the small amount of "backwater," the peak value of the water height on the deck at PH3 was hardly affected in the current encounter period. Therefore, Case 1 formed one significant peak.

When the wave steepness was larger than 0.050, the total amount of water on the deck increased, and the amount of "backwater" returning from the top of the wave baffle to the bow also increased. The "backwater" formed in the last encounter period will meet the green water opposite the "backwater" direction at PH3 in the current encounter period, as depicted in Figures 20(a) and (b). The "backwater" increased the height of the green water H_{GW}. Therefore, Case 2 and Case 3 formed the second peak after the first peak of the water height on the deck was formed.

However, in Case 4, the "backwater" in the last encounter period has a greater impact on the peak of H_{GW}. The "backwater" impacted the green water in the current encounter period, as depicted in Figure 20(c). The amount of "backwater" is greater in Case 4 than in Case 2 and Case 3. Therefore, after the formation of the first peak, the second peak of H_{GW} was stimulated, which is larger than the first peak.

The analysis shows that the wave steepness and "backwater" have a great impact on the value and number of the peak of water height on the deck.

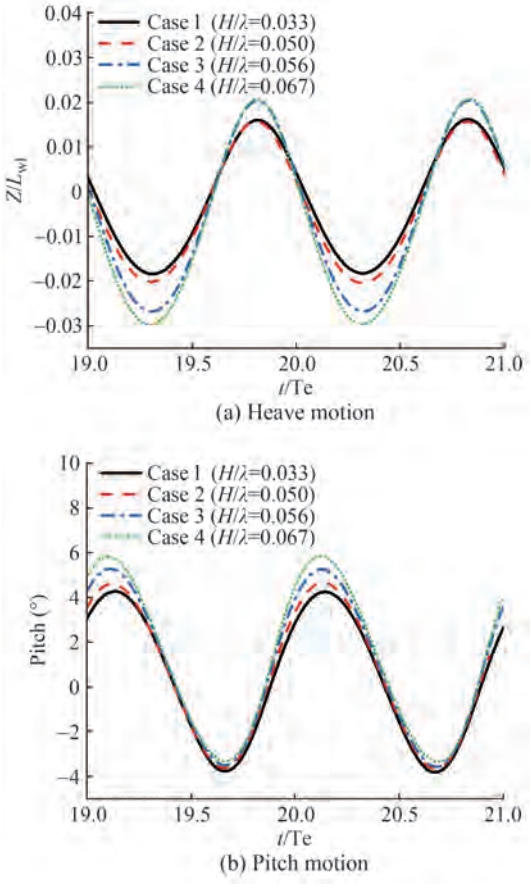

Figure 17 Time history of the ship motion

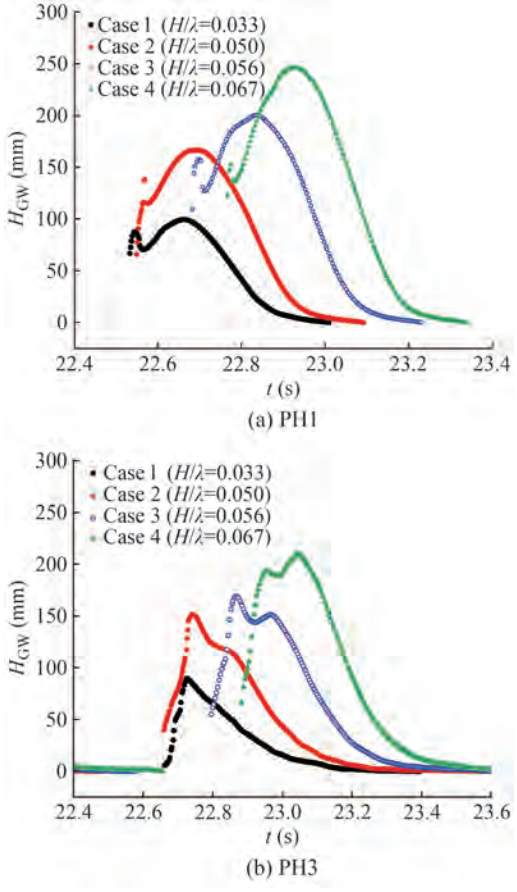

Figure 18 Time history of the water height on the deck

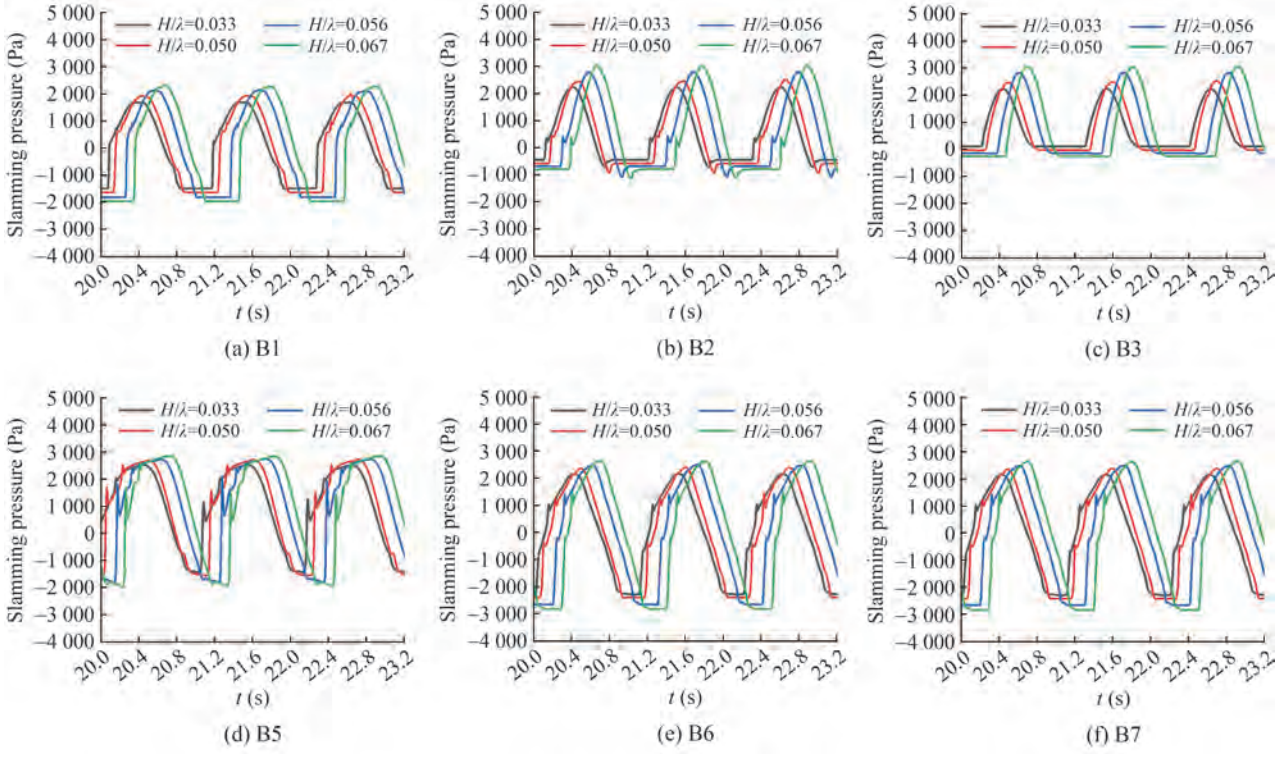

Figure 19 Time history of the slamming pressure

5.3 Influence of the wave height on impact loads

B1–B3 and B5–B7 were selected to evaluate the influence of the wave height on the impact loads at the side and bottom of the bow. The time history of the slamming dynamic pressure is depicted in Figure 19.

When the wave steepness increased from 0.050 to 0.056, the crest value of the slamming pressure significantly increased at B1–B3. B3 had the largest increase at the bow side in Case 3, approximately 20.83%, compared with Case 2.

The time history curves of B3 are smoother compared with those of B1 and B2 at the bow side. This is because B3 is at the low-tumblehome freeboard. Different from the bow-flare slamming, the pressure of B3 did not sharply increase in a very short time, but it smoothly increased in the process of the bow entering the water. Hence, the tumblehome vessel can effectively avoid the sudden increase of pressure at the freeboard.

Figure 19(d), (e), and (f) demonstrate that the slamming pressure sharply increased at the bottom of the bow. In particular, at station 0, the B5 slamming pressure increased by approximately 4 000 Pa in a moment. Large wave steepness caused the water entry and exit from the bow.

Compared to the ship side, the slamming pressure at the bottom of the bow changed more violently in a very short time when the ship entered the water.

5.4 Dynamic process and "wave run-up" of green water

Figures 20–24 depict the green water of the wave-facing tumblehome hull at four stages under a large wave steepness during an encounter period. The dynamic process and "wave run-up" of the green water were evaluated.

During the first 1/4 encounter period (20.00Te–20.25Te), when the crest of waves reached the ship bow in Case 2, there is no water on the deck behind the wave baffle at t = 20.00Te, as depicted in Figure 20(a). However, in Case 3, Figure 20(b) depicts that there is a large amount of water on the deck left from the previous encounter period behind the wave baffle at t = 20.00Te. When H/λ was 0.067, the deck area covered by water increased, and water even appeared on the deck at the stern, as depicted in Figure 20(c). Meanwhile, the "wave run-up" process is still in progress at t = 20.00Te. At the end of the first 1/4 encounter period (t = 20.25Te), the water surged onto the deck, and the water body was concentrated in the area from the bow to the wave baffle, as depicted in Figures 21(a)–(c).

Hence, when H/λ increases to 0.056, even if there is a wave baffle with a 20° inclination, it will still lead to serious water accumulation on the deck.

In the second 1/4 encounter period (20.25Te–20.50Te), in Case 2, the water on the deck continuously flowed out to the ship side, reducing the total amount of water on the deck, as depicted in Figure 22(a). Compared with Case 2, the total amount of water on the deck increased at t = 20.50Te in Case 3, as depicted in Figure 22(b). In Case 4, the amount of water at the wave baffle significantly increased. Meanwhile, a large amount of water flowed out to the ship side due to the obstruction of wave baffles. The water body tends to climb over the wave baffle at the end of the second 1/4 encounter period, as depicted in Figure 22(c).

In the third 1/4 encounter period (20.50Te–20.75Te), in Case 2, when a water body was obstructed, water parallel to the wave baffle was formed. The water body climbed to the top of the wave baffle, exhibiting the "wave run-up" phenomenon at t = 20.75Te, as depicted in Figure 23(a). However, in Case 3, the large trim amplitude by the stern accelerated the impact of water on the wave baffle. Compared with Case 2, the water body thickness at the wave baffle was significantly increased. The water climbed up and exhibited a plunging trend on the top of the wave baffle at t = 20.75Te, as depicted in Figure 23(b). When H/λ was 0.067, the height of the "wave run-up" was higher than that of Case 3, as depicted in Figure 23(c).

In the last 1/4 encounter period (20.75Te–21.00Te), in Case 2, the "wave run-up" process ended. As the hull inclined toward the bow, a part of the water attached to the wave baffle returned to the deck and formed water on the deck at t = 21.00Te, as depicted in Figure 24(a). In Case 3, the plunging water body slapped on the deck behind the wave baffle. However, the "wave run-up" process is still in progress in Case 4. Figure 24(c) depicts that the water accumulation on the deck behind the wave baffle was more serious. The water on the deck was utilized in the next green water period.

6 Conclusions

In this study, the green water of a wave-facing tumblehome vessel at Fr = 0.22 was simulated under strong nonlinear regular waves ($0.033 \leqslant H/\lambda \leqslant 0.067$). The motion response, water height on the deck, dynamic process of the green water, and "wave run-up" phenomenon were evaluated under different large wave steepness. The main conclusions are as follows:

1) The predicted time history of the water height on the deck and slamming pressure was verified with the experimental results under H/λ = 0.05. This finding proves the applicability of the CFD method for simulating green water under large wave steepness.

2) When H/λ increased from 0.050 to 0.056 at Fr = 0.22, the amplitude of the heave motion and trim by the bow increased by approximately 30% and 14.57%, respectively. The change in the water height on the deck was most obvious when H/λ increased from 0.033 to 0.050. However, the wave height had little effect on the green water duration. In addition, the wave steepness and "backwater" have a great impact on the value and number of the peak of water

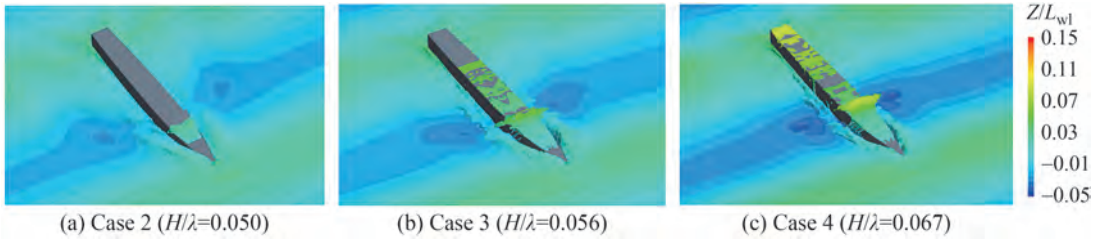

Figure 20 Green water at t = 20.00Te

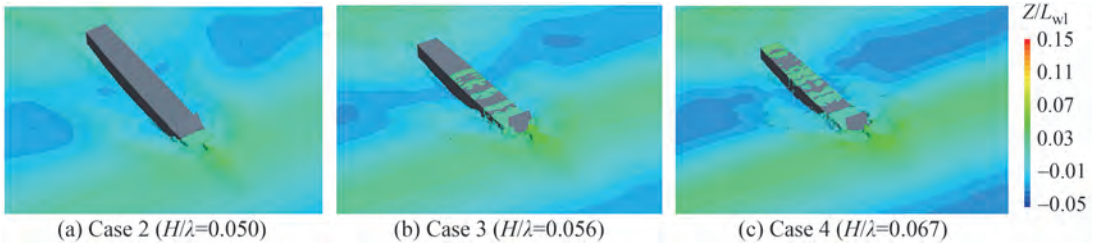

Figure 21 Green water at t = 20.25Te

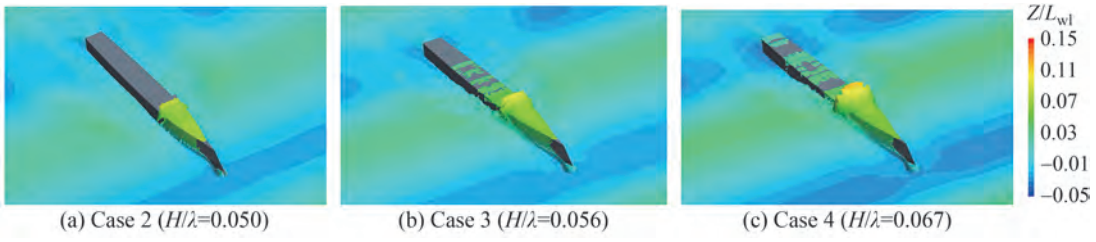

Figure 22 Green water at t = 20.50Te

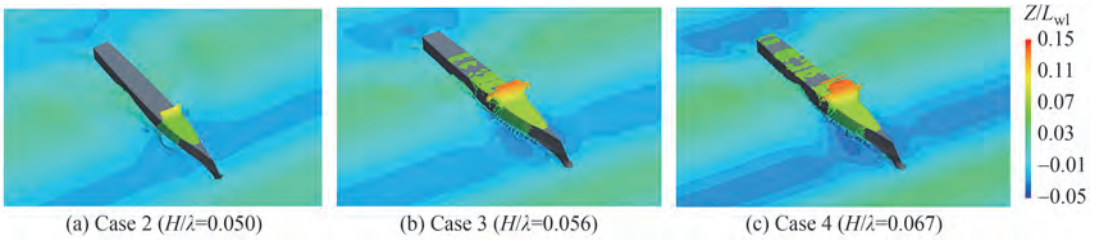

Figure 23 Green water at t = 20.75Te

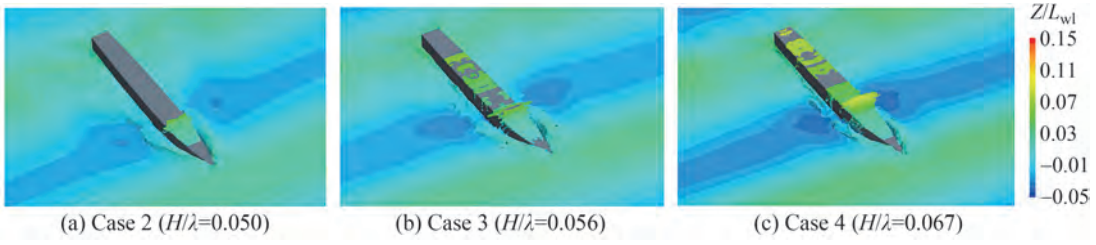

Figure 24 Green water at t = 21.00Te

height on the deck.

3) The tumblehome vessel can effectively avoid the sudden increase of slamming pressure at the freeboard. Compared to the ship side, the slamming pressure at the bottom of the bow sharply increased. At the bottom of station 0, when H/λ is 0.056, the slamming pressure increased by approximately 4 000 Pa in a very short time.

4) The "wave run-up" in all three cases occurred in the third 1/4 encounter period. As the wave steepness increased to 0.056, the water climbed up, and a plunging-type water

body was formed at the top of the wave baffle, causing a large water area on the deck. Meanwhile, an increase in the wave height will lead to the prolongation of the "wave run-up" duration.

This study offers value in terms of the prediction of green water in tumblehome vessels in extreme sea waves. In the future, more evaluations are required on the influence of wavelength, wave baffle shape, and inclination angle on green water.

Funding Supported by the Heilongjiang Touyan Project of China, and the Frontier Science Center of the Ministry of Education for Extreme Marine Environment Wave Fields.

Acknowledgement The authors would like to thank Prof. Hui Li and Prof. Shuzheng Sun for providing experiment data on the tumblehome vessel model.

References

Baquet A, Kim J, Huang Z (2017) Numerical modeling using CFD and potential wave theory for three-hour nonlinear irregular wave simulations. Proceedings of the ASME 2017 36th International Conference on Ocean, Offshore and Arctic Engineering, Trondheim, Norway, V001T01A002. https://doi.org/10.1115/OMAE2017-61090

Berhault C, Guerin P, Martigny D, Guert R (1998) Experimental and numerical investigations on the green water effects on FPSOs. Proceedings of the 8th International Offshore and Polar Engineering Conference, Montreal, Canada, ISOPE-I-98-043

Deng JW, Guo XX, Yang JM, Li X (2021) Experimental investigation on flow and load characteristics of green water onto FPSO under large wave steepness. Ship Engineering 43(6): 128-134. (in Chinese) https://doi.org/10.13788/j.cnki.cbgc.2021.06.23

Duan WY, Wang RF, Ma S, Chen YS (2013) Model test of green water of ships in regular waves. Journal of Harbin Engineering University 34(10): 1209-1213, 1260. (in Chinese) https://doi.org/10.3969/j.issn.1006-7043.201211042

Fenton J (1985) A fifth-order Stokes theory for steady waves. Journal of Waterway Port Coastal and Ocean Engineering-ASCE 111: 216-234. https://doi.org/10.1061/(ASCE)0733-950X(1985)111:2(216)

Gao H, Zhang ZG (2016) Research on two-dimensional model experimental on green water. Ship Engineering 38(8): 54-57, 70. (in Chinese) https://doi.org/10.13788/j.cnki.cbgc.2016.08.054

Goda K, Miyamoto T (1976) A study of shipping water pressure on deck by two-dimensional ship model tests. Journal of the Japan Society of Naval Architects & Ocean Engineers 1976(140): 16-22. https://doi.org/10.2534/JJASNAOE1968.1976.140_16

Gong C, Zhu RC, Miao GP, Fan J (2014) A numerical method of the simulation of green water on the deck of a vessel. Journal of Ship Mechanics 18(5): 524-531. (in Chinese) https://doi.org/10.3969/j.issn.1007-7294.2014.05.006

Gerco M (2001) A two-dimensional study of green-water loading. PhD thesis, Norwegian University of Science and Technology, Trondheim, 31-46

He GH, Zhang ZH, Wang ZK, Qi C (2018) Time-domain simulation of large-amplitude motion and green water loading of Wigley hull. Journal of Harbin Engineering University 39(8): 1269-1277. (in Chinese) https://doi.org/10.11990/jheu.201702047

He WZ, Dai YS, Xie N, Gao HQ, Zhou ZQ (1996) Statistical evaluation of green water occurrence in prediction of deck wetness for ships. Shipbuilding of China 1996(3): 1-12. (in Chinese)

Kim J, O'Sullivan J, Read A (2012) Ringing analysis of a vertical cylinder by Euler overlay method. Proceedings of the ASME 2012 31st International Conference on Ocean, Offshore and Arctic Engineering, Rio de Janeiro, 855-866. https://doi. org/10.1115/OMAE2012-84091

Li H, Deng BL, Ren HL, Sun SZ (2020) Investigation on the nonlinear effects of the vertical motions and vertical bending moment for a wave-piercing tumblehome vessel based on a hydro-elastic segmented model test. Marine Structures 72: 102757. https://doi.org/10.1016/j.marstruc.2020.102757

Liang XF, Yang JM, Li J, Yang C, Li X (2010) Numerical study of water behavior in green water occurrence. The Ocean Engineering 28(2): 29-36. (in Chinese) https://doi. org/10.3969/j. issn. 1005-9865.2010.02.005

Liu DY, Li FZ (2020) Numerical simulation of green water on Freak Waves. Shipbuilding of China 61(S2): 18-26. (in Chinese) https://doi.org/10.3969/j.issn.1000-4882.2020.z2.003

Liu L (2017) The longitudinal motion of tumblehome hull with speed and viscous numerical simulation of green water. Master thesis, Wuhan University of Technology, Wuhan, 67-76

Ochi MK (1964) Extreme behavior of a ship in rough seas. Annual Meeting of the Society of Naval Architects and Marine Engineers, New York, 143-202

Ogawa Y, Taguchi H, Ishida S (1997) Experimental study on shipping water volume and its load on deck. Journal of the Society of Naval Architects of Japan 1997(182): 177-185. https://doi. org/10.2534/JJASNAOE1968.1997.182_177

Ogawa Y, Taguchi H, Ishida S (1998) A prediction method for shipping water height and its loads on deck. Developments in Marine Technology 11: 535-543. https://doi. org/10.1016/S0928-2009(98)80195-9

Rosetti G, Pinto M, De Mello P, Sampaio C, Simos A, Silva D (2019) CFD and experimental assessment of green water events on an FPSO hull section in beam waves. Marine Structures 65: 154-180. https://doi.org/10.1016/j.marstruc.2018.12.004

Stansberg CT, Karlsen SI (2001) Green sea and water impact on FPSO in steep random waves. Practical Design of Ships and Other Floating Structures 1: 593-601. https://doi.org/10.1016/B978-008043950-1/50075-2

Sun SZ, Du WL, Li H (2017) Study on green water of tumblehome hull using dambreak flow and RANSE models. Polish Maritime Research 24(s2): 172-180. https://doi.org/10.1515/pomr-2017-0080

Tasaki R (1960) On the shipping water in head waves. Journal of Zosen Kiokai 1960(107): 47-54. https://doi. org/10.2534/jjasnaoe 1952.1960.107_47

Wang RK, Wu JP (1998) Calculation for the wetness curve and the statistical properties of green water on deck. Journal of Wuhan University of Technology (Transportation Science & Engineering) 1998(1): 10-14. (in Chinese)

Xu C, Tang WY (2018) Numerical simulation of green water on deck and analysis of the entrapped air. Ship & Ocean Engineering 47(1): 6-10. (in Chinese) https://doi. org/10.3963/j. issn. 1671-7953.2018.01.002

Yang ZW, Sun L, Wang SH, Fang ZR, Li JS (2021) Analysis of complex flow field of green water on FPSO. Journal of Wuhan University of Technology 45(6): 1068-1073. (in Chinese) https://doi.org/10.3963/j.issn.2095-3844.2021.06.012